

CDC-42 encodes dynamically stable asymmetries in the *C. elegans* zygote via an incoherent feed-forward loop

Ondrej Maxian, Cassandra Azeredo-Tseng, Alex Anneken, Chris Schoff, Howard Clark,
and Edwin Munro

April 30, 2024

Introduction

Cell polarity is essential for many aspects of organismal development and physiology, including stem cell dynamics, directional cell migration, and asymmetric cell division (Dewey et al., 2015; Goldstein and Macara, 2007; Ierushalmi and Keren, 2021; Maître et al., 2016). For most cells, the first step in polarization involves a symmetry-breaking response to a transient localized cue that creates asymmetric distributions of specific molecules or molecular activities. The mechanisms that underlie cellular symmetry-breaking have been extensively explored (Li and Bowerman, 2010), but mechanisms that maintain polarity as a dynamically stable state with a fixed boundary position have only recently come under scrutiny (Sailer et al., 2015; Gross et al., 2019).

On a large scale, a cell’s polarity state is encoded by asymmetric distributions of protein molecules, which are shaped by smaller-scale processes like binding, diffusion, and active transport. In *C. elegans*, polarity is encoded by the distribution of two distinct groups of (highly conserved) polarity proteins: anterior PARs (aPARs), which include the scaffold PAR-3, adaptor PAR-6, atypical kinase PKC-3, and GTPase CDC-42, and posterior PARs (pPARs), which include the RING-domain containing protein PAR-2 (Bland et al., 2023), kinase PAR-1, tumor suppressor LGL-1, and CDC-42 GAP CHIN-1 (Lang and Munro, 2017).

Wild-type embryos polarize in two distinct phases termed “establishment” and “maintenance” (Fig. 1a, Cuenca et al. (2003)). The mechanisms that underlie symmetry-breaking during polarity establishment have been well-studied (Cowan and Hyman, 2007; Munro and Bowerman, 2009; Gross et al., 2019; Reich et al., 2019). Near the end of meiosis, PAR-3, PAR-6 and PKC-3 are uniformly distributed at the cortex, where they prevent cortical association of PAR-1, PAR-2 and LGL-1

(Schonegg and Hyman, 2006; ?). One mode of symmetry-breaking involves the local inhibition of actomyosin contractility near the sperm MTOC, which triggers cortical flows that transport F-actin, myosin II, PAR-3/PAR-6/PKC-3, and other cortically associated factors towards the anterior pole, resulting in their mutual restriction to an anterior cap (Munro et al., 2004; Rodriguez et al., 2017). Posterior depletion of PAR-3/PAR-6/PKC-3 then allows PAR-1, PAR-2 and LGL-1 to associate with a complementary posterior domain. Actomyosin contractility and cortical flow during polarity establishment require the small GTPase Rho-1 (Schonegg and Hyman, 2006; Motegi and Sugimoto, 2006), and in fact the sperm cue acts via Aurora A kinase (AIR-1) to locally inhibit Rho through the Rho GEF Ect-2 (Motegi and Sugimoto, 2006; Tse et al., 2012; Longhini and Glotzer, 2022; Kapoor and Kotak, 2019). AIR-1 has also been linked to activation of the PAR network, which prevents spontaneous polarization earlier in the cell cycle (Reich et al., 2019), and to a second mode of symmetry-breaking in which sperm astral microtubules promote local association of Par-2 with the posterior cortex (Motegi et al., 2011; Klinkert et al., 2019; Manzi et al., 2024).

While the mechanisms that break symmetry are by now well understood, it remains unclear what *stops* symmetry breaking. If the system is programmed to amplify an initial polarizing cue, what sets the limit of amplification? The by now standard mechanism is that anterior (CDC-42/PAR-3/PAR-6/PKC-3) and posterior proteins (PAR-1/PAR-2/LGL-1) form a bistable reaction diffusion system by competing for residence at the cortex/plasma membrane such that one or the other but not both win locally. Theoretical studies suggest that in principle such a mechanism could stabilize the AP boundary after establishment phase cortical flows cease, or in embryos that lack cortical actin or myosin (Mori et al., 2008; Dawes and Munro, 2011; Goehring et al., 2011; Lang et al., 2023). Without flows, however, the A/P boundary cannot shift on a realistic timescale by diffusion alone (Lang et al., 2023). Consequently, biochemistry cannot explain the tendency of maintenance to correct errors from establishment (Zonies et al., 2010), which is a process we study in more depth in this work.

In the presence of flow, it is still unknown what sets a limit to boundary progression. Recent work showed that, assuming an intrinsic self limit to contractility, the boundary can be pinned (Gross et al., 2019), with the position set by the total amount of each PAR protein (Goehring et al., 2011). The specific assumption used in (Gross et al., 2019) was that contractility is saturated during maintenance phase (even in the posterior), meaning there are no flows. But previous maintenance-phase studies have reported noticeable myosin flows from the posterior half of the embryo into an anterior cap where myosin is enriched (Sailer et al., 2015). Despite this steady flow, the

cap does not contract (Sailer et al., 2015). Moreover, ectopic accumulation of Myosin II during maintenance in PAR-2 mutants is associated with abnormal posterior-directed cortical flows and rapid redistribution of Par proteins (Munro et al., 2004), suggesting that the distribution of myosin, in addition to the PAR proteins, guides the steady state. Thus it remains a mystery how the cell could dynamically stabilize a boundary in the presence of a myosin (contractile) asymmetry, and a nonzero pattern of flow.

While we will show that the self-limiting nature of contractility applies in both establishment and maintenance phase, our focus in particular will be on maintenance, which requires CDC-42 to maintain asymmetries set up during establishment (Kay and Hunter, 2001; Gotta et al., 2001; Aceto et al., 2006; Schonegg and Hyman, 2006; Motegi and Sugimoto, 2006). GFP-tagged CDC-42 becomes anteriorly enriched during polarity establishment, and studies with a GFP-tagged biosensor suggest that the active (GTP-bound) form of CDC-42 may be similarly enriched during maintenance phase (Kumfer et al., 2010). Binding of CDC-42 to the conserved semi-Crib domain of PAR-6 is required for cortical association of PAR-6/PKC-3 during maintenance (Aceto et al., 2006), and PKC-3 is in an active state only when bound to CDC-42 (Sailer et al., 2015; Lang and Munro, 2017; Rodriguez et al., 2017). CDC-42 also acts through MRCK-1, a *C. elegans* orthologue of the mammalian Myotonia Dystrophy-related CDC-42-binding kinase MRCK, to promote asymmetric cortical recruitment of myosin II (Kumfer et al., 2010). There is also evidence that CDC-42 promotes asymmetric enrichment of F-actin during maintenance phase (REF?), but the underlying mechanism remains poorly understood. More generally, it remains unclear how these distinct outputs of CDC-42 are integrated to dynamically stabilize the AP boundary at a fixed axial position and limit contractility.

In this study, we combine experiments and theoretical modeling to show that boundary progression can be stalled when distinct outputs of CDC-42 have different effects on contractility. By extending both establishment and maintenance phases, we show that the boundary position is in fact stable, regardless of the cell cycle phase. We then demonstrate, through mutations that affect establishment phase, that the steady state observed at the end of maintenance phase is independent of what happens in establishment (if cortical flows are not blocked). This reveals that maintenance phase is essentially an error correction mechanism which encodes a dynamically stable attractive state.

To understand how the PAR protein circuit (which involves CDC-42) interacts with myosin contractility to limit the extent of contractility, we introduce a mathematical model. Without a self-

limiting character to the flow, the boundary either contracts all the way to the end of the embryo, or slowly moves to the embryo interior over a timescale an order of magnitude longer than maintenance phase. To find the missing model component, we return to experiments, which demonstrate that branched actin in the anterior acts to reduce tension and prevent excessive contraction, similar to behavior observed previously in other systems (Muresan et al., 2022; Yang et al., 2012). Our model reveals that adding a threshold of CDC-42, above which branched actin is produced, can successfully reproduce the dynamics of maintenance phase. We find the key contribution of branched actin is to decouple enrichment of anterior PARs (which prevent the pPAR domain from expanding) from the increase in contractility and flow speeds (which expand the pPAR domain). When contractility stalls, mechanisms based on reaction-diffusion (Mori et al., 2008; Goehring et al., 2011) are effective in stabilizing the boundary.

Results

Establishment and maintenance phase contractility are governed by unique biochemical systems

As a first step to examining the role of CDC-42 in regulating contractility, we sought to distinguish the phases of the cell cycle in terms of their upstream myosin regulator. We began by imaging wild-type embryos expressing non-muscle myosin II fused to GFP (NMY-II::GFP), as well as embryos expressing PAR-6::GFP. At pseudo-cleavage and prior to the onset of centration (Fig. 1A), myosin exhibited pulsatile dynamics, with large foci appearing and disappearing over time, and PAR-6 was enriched in clusters on the anterior cortex (Fig. 1B). By nuclear envelope breakdown, both myosin and PAR-6 had transitioned to diffuse, smaller clusters enriched on the anterior cortex (Fig. 1B). Pulsatile myosin activity during establishment phase has previously been shown to involve rho-mediated contractility (Michaux et al., 2018; Michaud et al., 2022; Yao et al., 2022), while the diffuse myosin clusters have been previously linked to CDC-42 (Motegi and Sugimoto, 2006). Likewise, previous reports (Motegi and Sugimoto, 2006; Rodriguez et al., 2017) have shown that the diffuse PAR-6 clusters are correlated with binding to CDC-42, which activates PKC-3, while the punctate clusters of PAR-6 are associated with PAR-3. We therefore conclude that Rho-1 mediates contractility during polarity establishment phase, while CDC-42 controls both contractility and PAR polarity during maintenance phase. The coupling of biochemistry and contractility through CDC-42 makes maintenance unique relative to establishment.

To understand the markers of the transition from establishment to maintenance, we depleted embryos of PRI-1 via RNAi, which prevented DNA replication and stalled cells in late establishment phase. In particular, we found a typical delay time of about eight minutes from pronuclear meeting to centration onset, relative to wild type embryos (Fig. 1C, D). The delay in centration onset also correlated with a delay in pseudo-cleavage relaxation (Fig. 1C), as well as a delay in the myosin transition from punctate to diffuse (Fig. 1D). These events consequently mark the transition from establishment to maintenance, and especially to the regime of CDC-42-mediated contractility. While this regime is our interest here, it is noteworthy that embryos in late establishment phase (especially PRI-1 depleted embryos) exhibit a stable A/P myosin asymmetry characterized by persistent anterior-directed flow, similar to previous observations for maintenance phase. We return to this point in the discussion.

The maintenance phase steady state is unique and attractive in the presence of MRCK

Previous studies Sailer et al. (2015) have studied the dynamics of maintenance phase in wild type embryos in considerable detail. After pseudocleavage relaxation, embryos exhibit a period of “posterior contraction,” where active CDC-42 on the posterior cortex drives flows which transport myosin to the posterior (Fig. 2A). The posterior CDC-42 activity is transient, however, and following a period of about 80 s embryos transition to a state of persistent anterior-directed flow, with both CDC-42 and myosin preferentially enriched on the anterior cortex (Fig. 2A). Both phases of flow are abolished by depleting the kinase MRCK, which acts downstream of CDC-42 to activate myosin.

We first wanted to understand if the boundary position is a function of previous dynamics during establishment phase, or if the basic ingredients of maintenance phase contractility (CDC-42 and MRCK) are sufficient to set the boundary position and flow profile independently. To this end, we systematically imaged symmetry breaking in temperature-sensitive ect-2 mutants, which fail to activate rho during establishment phase and therefore do not polarize. We marked the beginning of maintenance phase via the appearance of myosin clusters, and the end of maintenance phase as the onset of embryo rotation prior to cytokinesis.

As described in previous reports (Zonies et al., 2010), ect-2 mutant embryos exhibited symmetry breaking that we refer to as “maintenance phase rescue,” since it occurs only when myosin is distributed in diffuse clusters (Fig. 2A). During rescue, myosin and anterior PAR proteins segregated into an anterior domain of the same size as observed in late maintenance phase in wild-type embryos

(Fig. 2B). At the end of rescue, the pattern of flow was characterized by a stronger flow in the posterior half of the cell into a stall point at the edge of the anterior cap, as in late maintenance wild type embryos (Fig. 2B). Embryos depleted of the kinase MRCK, which acts downstream of CDC-42 to activate myosin, failed to rescue polarity in maintenance phase, as neither the anterior PAR domain nor myosin domain contracted towards the anterior (Fig. 2C). We conclude that rescue in ect-2 ts mutants is driven by CDC-42-mediated contractility (through MRCK), which is specific to maintenance phase.

Having characterized maintenance phase dynamics when establishment phase is either totally effective or totally ineffective, we wondered if having partial polarity establishment would lead to partial polarity rescue. To accomplish this, we performed experiments in NOP-1 mutants, which display partial degrees of establishment-phase contractility because of partial rho activation (Tse et al., 2012). The establishment phase boundary position therefore varied from embryo to embryo. Upon the transition to maintenance phase in these embryos, cortical flows were initiated, and the boundaries in each of the cells converged to the same approximate position at roughly 60% embryo length (Fig. 2D). By contrast, in the absence of MRCK, the A/P boundary stayed in the same position throughout maintenance phase, and no cortical flows were initiated (Fig. 2D). We conclude that partial polarity establishment leads to partial rescue in the presence of MRCK.

We note that previous studies in ect-2 mutants have reported a delayed symmetry breaking (Zonies et al., 2010; Tse et al., 2012), but have not directly explained this as a maintenance-phase phenomenon, nor studied how the boundary position and flow profile change relative to late maintenance phase in the wild type. Our data clearly show that rescue in establishment-defective mutants is driven by an activation of maintenance phase contractility (CDC-42 acting through MRCK), and that this contractile circuit combines with the PAR circuit to encode a unique state at the end of maintenance phase.

The steady state of maintenance phase is a stable boundary with persistent anterior-directed flow

We next wondered whether the state observed in late maintenance is a true “steady state,” or if the myosin asymmetry and anterior-directed flow would eventually cause further contraction of the anterior domain. To probe this, we extended maintenance phase by depleting wild-type embryos of the cell cycle regulator CDK-1. Marking maintenance phase as the period between pseudocleavage relaxation and anaphase onset, we obtained a window of roughly 8–10 minutes per cell, in which

we characterized the myosin intensity and flow speeds. Later stages of the extended maintenance phase showed a relatively stable position of the myosin boundary (it in fact expanded towards the posterior slightly) and a persistent anterior-directed flow which tends to achieve a maximum (magnitude) just posterior of the peak myosin location (Fig. 2E,F). However, because the myosin intensity and flow speeds in CDK-1 (RNAi) never resemble those of wild-type, it is clear that interfering with CDK-1 affects more than just the cell cycle, and it is impossible to say concretely that the specific flow and myosin profiles in late maintenance are “steady.” Nevertheless, we can conclude that an asymmetric myosin profile and persistent anterior-directed flow do not lead to further contraction of the boundary when maintenance is extended.

Existing models cannot explain the dynamics of maintenance phase rescue

We next explored whether a mathematical model, informed by existing knowledge of maintenance phase, could explain how maintenance phase tends to correct errors from establishment and establish a steady state. We first considered whether the phenomenon of maintenance-phase rescue could be a consequence of an instability in the underlying myosin dynamics. Along this line, we performed linear stability analysis of a simple myosin model informed by our experimental data (Mayer et al., 2010; Bois et al., 2011). The stability analysis shows that the dynamics are unstable when the flow carries myosin molecules a distance larger than the hydrodynamic lengthscale, which is the typical length a local disturbance propagates through flows (Mayer et al., 2010). For realistic lifetimes on the order 5–20 s, the minimum flow speed to generate instability is about 40 $\mu\text{m}/\text{min}$, which is much faster than ever observed in maintenance phase. Thus the dynamics of maintenance phase rescue are not due to myosin instabilities.

Because the dynamics of myosin alone are insufficient to generate instability, PAR proteins must be essential for rescue to occur, as was previously shown in the case of PAR-2 (Zonies et al., 2010). We consequently studied a model of maintenance phase biochemistry based on previously-characterized interactions (Fig. 3A, Lang and Munro (2017)). On the anterior side, we introduced three distinct protein species: PAR-3, CDC-42, and PAR-6/PKC-3, while in the posterior we lumped all posterior PARs (PAR-2, PAR-1, and CHIN-1) into one species. A schematic diagram is given in Fig. 3A, and the equations which describe the circuit are given in the SI. In brief, PAR-3 is locally bistable because of oligomerization and positive feedback (Lang et al., 2023). The enriched zone of PAR-3 sets up a gradient of PAR-6/PKC-3, which inhibits all of the posterior PAR proteins. The posterior PARs then inhibit CDC-42 (directly through CHIN-1 and indirectly through PAR-2)

(Munro et al., 2004; Sailer et al., 2015).

In the absence of contractility, our model predicts that the maintenance phase circuit has a unique boundary position, where the PAR-3 boundary sits at about 50% embryo length (bottom right plot in Fig. 3B; see also the SI for a discussion of how this boundary position changes when PAR-3 is inhibited by PAR-1). Under normal circumstances, where the boundary begins at 50% embryo length (the end of establishment phase), it rapidly adjusts to its unique position in under ten minutes (top right panels in Fig. 3B). By contrast, under rescue conditions, which we simulated via a local loading of pPARs in the posterior-most 10% of the embryo, the boundary slowly corrects, taking about an hour to reach steady state (left panels in Fig. 3B). The steady state here is reached through a wave-pinning mechanism (Mori et al., 2008; Goehring et al., 2011), where the boundary stops moving when reaction and diffusion fluxes (both of which depend on the cytoplasmic protein concentration) come into balance. The change in protein concentration occurs through unbinding, which for most proteins occurs on the timescale of hundreds of seconds (Robin et al., 2014), thus explaining the slow dynamics. Our model therefore confirms the experimental result that rescue is impossible without flows (Fig. 2C).

To model contractility, we made CDC-42 a promoter of myosin at the cortex, and cortical tension directly proportional to myosin (blue parts in Fig. 3A, see SI for equations). We set up flows in the direction of gradients in cortical tension, with all proteins on the cortex advected with the local cortical velocity (Illukkumbura et al., 2023). With contractility, simulations under rescue conditions reproduce the initial stages of rescue (Fig. 3C), where an initially peaked profile of pPARs invades the anterior domain, concentrating aPARs in the middle and thereby increasing the concentration of pPARs in the posterior. As a result of this, CDC-42 gets inhibited in the posterior, which gives a gradient of myosin from posterior to anterior. The gradient of myosin generates a flow which further compacts the anterior domain. The timescale of this compaction is much faster than without flows, and indeed occurs on a timescale of minutes and not hours.

While this model reproduces the initial stages of the rescue process, adding contractility changes how the system responds to the enrichment of aPARs on the anterior. In particular, the reaction-diffusion mechanism that sets the boundary position in the absence of flow is no longer valid because enrichment of aPARs also enriches myosin. Thus, when the aPAR concentration increases, pPARs are still driven off the membrane at a higher rate, but pPARs are also advected into the boundary at a higher rate. The additional advective flux of pPARs overwhelms the increasing reactive flux, resulting in an ever-contracting boundary with ever-increasing flows and pPARs becoming uniformly

enriched (Fig. 3C). In order to properly reproduce rescue, the model suggests a need for a local inhibitor of contractility. If an additional agent can inhibit contractility without inhibiting other aPAR proteins, the reactive flux and advective flux would decouple, and the reaction-diffusion mechanism can stall the boundary. We return next to experiments to find such an inhibitor.

Branched actin reduces contractility in the anterior cortex

To determine where the missing ingredients are in the model, we looked for a contractile asymmetry across the A/P boundary. Using velocity data from late maintenance phase in wild type embryos, we used a simple active fluid model (Mayer et al. (2010) and SI) to extract a profile of stress, which we compared directly to the measured myosin intensity on the cortex (Fig. 4A). While there was perfect agreement between stress and myosin on the posterior, in the anterior there was a noticeable mismatch, with the gradient in stress being smaller predicted from the myosin profile. The reduction in anterior stress, combined with localization of branched actin in the anterior, suggests that branched actin might be responsible for inhibiting contractility there.

Previous studies in other systems (Yang et al., 2012; Muresan et al., 2022) have suggested that branched actin networks could constrain myosin mini-filament motion, thereby inhibiting contractility. To see if this mechanism could also be at work in the *C. elegans* zygote, we first compared F-actin organization in fixed, phalloidin-stained wild type and CDC-42-depleted embryos (Fig. 4B). In all embryos, a loose network of long filaments or filament bundles extended throughout the posterior cortex. Numerous bright puncta (hereon mini-comets) were enriched within the anterior cap, and a denser meshwork of filaments was also enriched within the anterior cap in a cortical layer superficial to the mini-comets.

Depletion of CDC-42 resulted in nearly complete loss of both mini-comets and the dense anterior meshwork, leaving a more uniform network of longer filaments/bundles (Fig. 4B) similar to that seen at the posterior cortex in the wild type. Thus, CDC-42 is required for localized assembly of a specific subset of filaments during maintenance. In other cell types, CDC-42 binds WASP family proteins to activate ARP2/3-dependent branched actin assembly (Pollitt and Insall, 2009). Consistent with this, depleting embryos of the essential ARP2/3 subunit ARX-2 caused a complete loss of both F-actin mini-comets and the dense anterior meshwork during maintenance, leaving the loose network of filaments similar to that seen at the posterior cortex in the wild type. Similarly, depleting embryos of the single *C. elegans* WASP homologue WSP-1 resulted in a severe reduction of the dense anterior mesh, although mini-comets remained highly enriched in the anterior cap (Fig.

4B). In the case of both *wsp-1* and *arx-2* RNAi, we observed a hyper-contractile anterior cap, with a reduction in cap size of about 15% embryo length (in *wsp-1* (RNAi)) and 25% embryo length (in *arx-2* RNAi). We conclude that CDC-42, acting through WASP, promotes the production of branched actin structures in the anterior which inhibit contractility.

To see if maintenance phase contractility also drives the hypercontractility we observe in *arx-2* depleted embryos, we performed live imaging of PAR-3::GFP in *arx-2* depleted embryos, with and without MRCK depletion. Our results showed a hypercontractile cap at the end of establishment phase. In embryos depleted of only *arx-2*, the cap continued to contract during maintenance. By contrast, embryos depleted of both *arx-2* and MRCK had caps which expanded during maintenance phase. We conclude that the same contractile circuit that drives rescue is also responsible for hypercontractility in these embryos. That is, two different targets of CDC-42, myosin (through MRCK) and branched actin (through WASP), combine to active and brake contractility, respectively.

To compare the dynamics of *arx-2* depleted embryos to our model without a contractile inhibitor, we performed live imaging of myosin dynamics in embryos depleted of *arx-2*. Unlike in wild type embryos, which formed a stable cap that remained steady in maintenance phase, embryos depleted of *arx-2* exhibited hypercontractility, with caps that tended to progress towards the anterior pole during maintenance phase (Fig. 4D). We tracked the myosin intensity during the three minutes prior to cytokinesis, finding a maximum intensity which progressively moved toward the anterior pole and grew over time (blue lines in Fig. 4E), in contrast to wild-type embryos, where the maximum myosin intensity retained a fixed position in the last three minutes of maintenance phase (red lines in Fig. 4E). Similar to the myosin intensity, we found the flow profile in *arx-2* (RNAi) embryos did not display a stall point near the anterior cap, but instead exhibited persistent anterior-directed flows throughout the whole embryo length (Fig. 4E) Indeed, repeating our previous experiment, in which we use the velocity profile during the last minute of maintenance phase to extract a stress and compare to the myosin profile, showed perfect agreement between myosin and stress across the entire embryo length in *arx-2* (RNAi) embryos (Fig. 4F). Thus, in wild type embryos branched actin must act in the anterior to inhibit contractility.

Our observations of the flow profile in *arx-2* (RNAi) embryos were somewhat confounded by their tendency to exhibit unstable rotation, leading to large bulk flows that were not aligned with the A/P direction. We hypothesized that these rotations could be caused by microtubule forces (from the mitotic spindle) pulling on the smaller anterior cap, which can no longer effectively resist them. Consistent with this, treating *arx-2* (RNAi) embryos with nocodazole, a drug which depoly-

merizes microtubules, removed the large-scale rotations and led to more consistent measurements of flow. The resulting myosin intensities and flow profiles (SI) were almost identical to those without nocodazole treatment, in that they exhibited a myosin peak which continuously shifted to the anterior, and a flow which was anterior-directed and on the order 2–4 $\mu\text{m}/\text{min}$ across the whole embryo length.

The dynamics of rescue suggest an activation threshold for branched actin

To further inform our model of branched actin, we looked at the dynamics of maintenance-phase rescue with and without branched actin. We first tested the effect of branched actin knockdown during maintenance phase rescue by depleting ect-2 (ts) embryos of arx-2 via RNAi. Unlike in normal rescue, where contraction of the anterior domain suddenly stalled, in embryos depleted of arx-2 the anterior domain appeared to contract at a constant rate until cytokinesis (Fig. 5A). The sudden stalling of the boundary in the presence of branched actin suggests a sudden production of branched actin on the anterior, which begins at a mid-point in the rescue process.

To further probe this idea, we systematically imaged the myosin intensities and flow profiles during rescue, with the average profiles every 30 seconds of rescue shown in Fig. 5B. We observed two distinct phases of rescue: in the first phase, the myosin intensity slightly increased, and the peak shifted towards the anterior. Meanwhile, flow speeds increased, with the peak in flow also shifting towards the anterior. After around three minutes, we observed a sudden decrease in flow speeds so that the flow profile matched the typical profile from late maintenance phase in wild type embryos (black line in Fig. 5B), which then stalled the myosin boundary at a fixed point near the typical wild-type boundary. Plotting the maximum myosin intensity and flow speeds, as well as the position of the maxima, over time during rescue revealed the order of events in the sudden stalling (Fig. 5C). First, the flow speed suddenly decreased, which led to the stalling of the myosin boundary, and finally the stalling of the flow boundary. All of this occurred without significant changes in the myosin profile (in particular the maximum myosin intensity). Thus, if branched actin is activated in the anterior midway through rescue, its role is to inhibit flow speeds, and not directly inhibit myosin. This observation forms the basis of our model in the next section.

Incorporating branched actin into existing models correctly reproduces rescue dynamics

We used our experimental observations about branched actin to reform our model (Fig. 6A). Based on the sudden transition of the flow speed during maintenance phase rescue, we hypothesized that branched actin is produced above a threshold of CDC-42 concentration, where the threshold is necessarily between the typical posterior and anterior levels of CDC-42. We assumed that, once produced, branched actin directly inhibits cortical tension (but not myosin). Flows are still in the direction of tension gradients, but now the tension profile depends on both myosin *and* branched actin (Fig. 6A).

Simulations that couple the model of branched actin with our previous model of PAR proteins and contractility (Fig. 3A) show stalled progression of the A/P boundary, with a final position that depends on the threshold of CDC-42 at which branched actin is produced (Fig. 6B). We quantified the threshold C_R in terms of the steady state anterior level of CDC-42 without contractility, C_A (Fig. 3B). When $C_R = C_A$, rescue proceeds as in the case without flows, but at $t = 10$ mins a sudden decrease in flows stalls boundary progression around 25% embryo length (top row of Fig. 6B; the bright dashed region in the CDC-42 kymographs is where the concentration is above the threshold). Decreasing the threshold to $C_R = 0.6C_A$ gives a similar phenomenon, but the boundary stalls sooner because CDC-42 crosses the threshold sooner (middle row of Fig. 6B). When the threshold is too small, rescue can never begin, because the CDC-42 concentration is (almost) everywhere above the threshold, causing branched actin to build up everywhere along the embryo length, thus inhibiting contractility everywhere (bottom row of Fig. 6B).

These simulations demonstrate that our existing knowledge about maintenance phase biochemistry, plus the actin of branched action through an incoherent feed forward loop involving CDC-42 (Fig. 6A) are sufficient to explain the dynamics of maintenance phase rescue, in particular the ability of the embryo to rapidly correct errors from maintenance without catastrophic build-up of contractility. In terms of reaction-diffusion dynamics, the role of branched actin is to decouple the build up of flows from the build up of anterior PARs. Once branched actin is active, the aPAR concentration (and reactive fluxes) can build up *without* flow speeds (advection fluxes) building up. Consequent build up of the aPARs then stalls the boundary via previously-described reaction-diffusion mechanisms (Mori et al., 2008; Goehring et al., 2011).

Discussion

We note a distinction here between maintenance and establishment phase. In the latter, instabilities in the dynamics of rho combine with delayed negative feedback to yield pulsatile dynamics (Nishikawa et al., 2017; Michaux et al., 2018; Michaud et al., 2022). The connection between these pulsatile dynamics and the large-scale flows that establish polarity is still unknown.

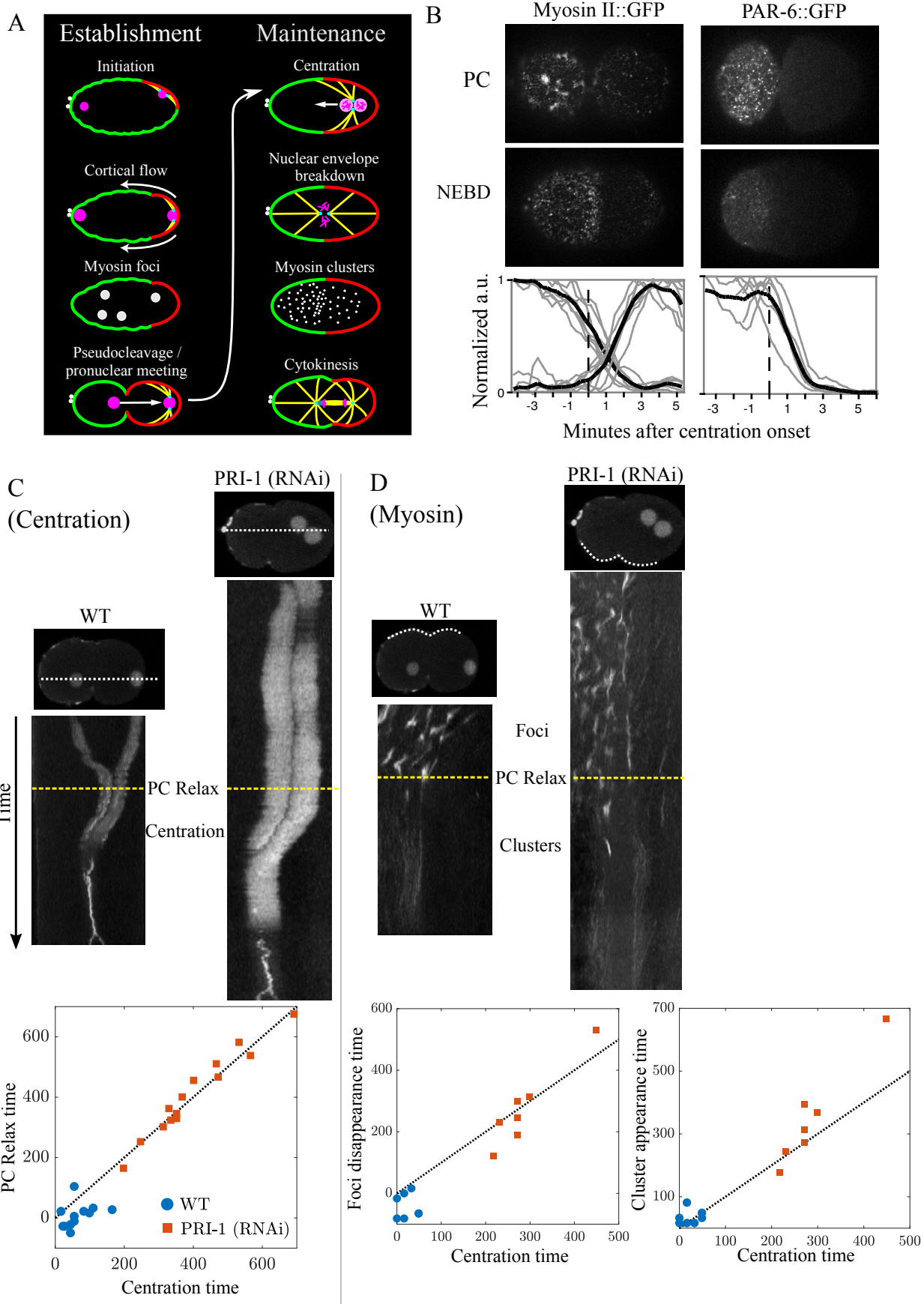
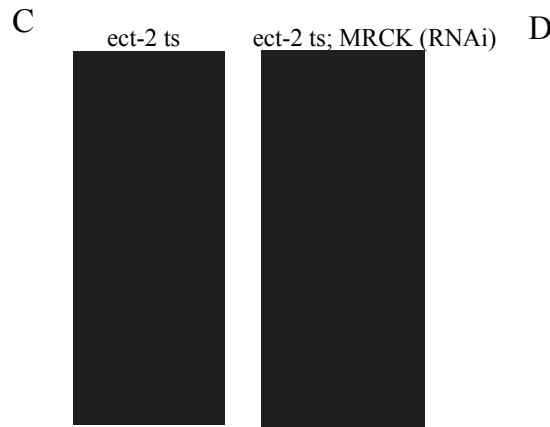
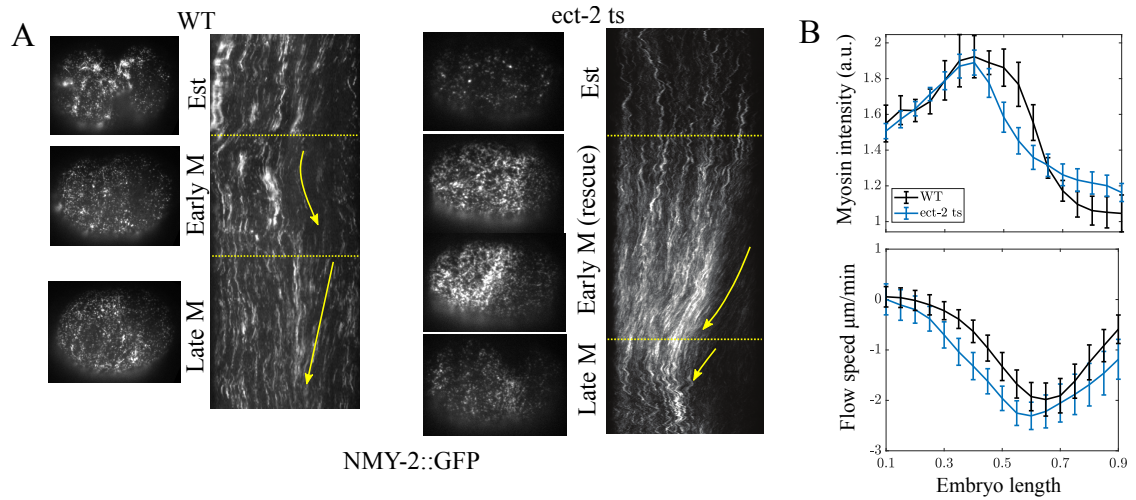


Figure 1: Cell cycle progression controls a regime change from rho-dependent to CDC-42-dependent contractility. (A) Overview of dynamics during establishment and maintenance phase, including key events in the cell cycle. (B) Surface views of non-muscle-myosin II (NMY-2::GFP; left panels) and GFP::PAR-6 (right panels) in wild-type embryos at/near the end of pseudocleavage (top panels) or nuclear envelope breakdown (bottom panels). Graphs show the normalized intensity of myosin foci and clusters (left), or PAR-6 clusters (right) over time relative to centration onset. (C) Kymographs and scatter plot showing the correlation between pseudo-cleavage relaxtion and centration onset in wild-type and PRI-1 (RNAi) embryos, where both are delayed. (D) Kymographs and scatter plots showing the correlation between myosin transitions, centration onset, and psuedo-cleavage relaxation in wild-type and PRI-1 (RNAi) embryos. Time in scatter plots is measured relative to pronuclear meeting.



Nop-1 expressing PAR-6 and PAR-2 +/- MRCK

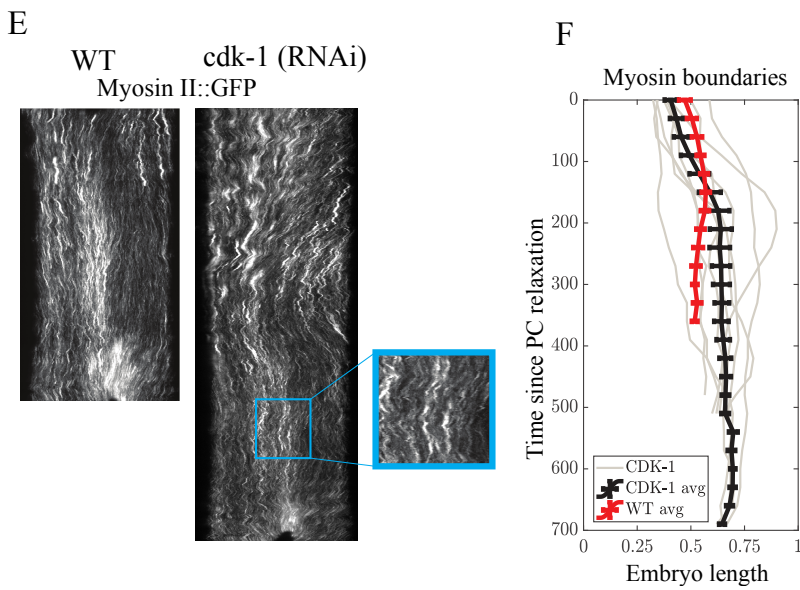
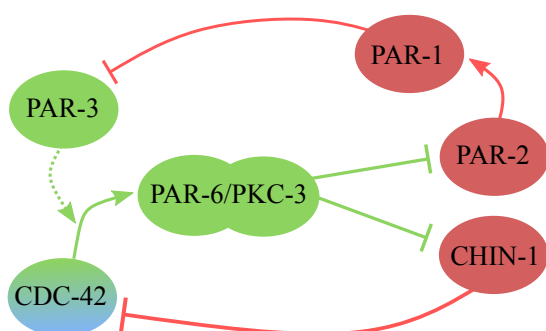


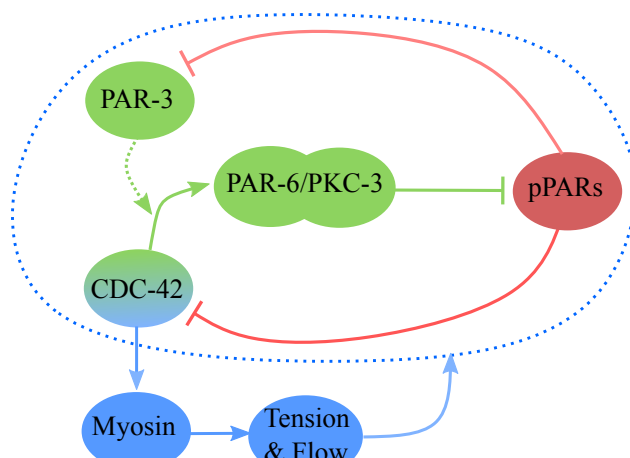
Figure 2: Maintenance phase encodes a stable, attractive steady state with a unique boundary position and flow pattern. (A) Dynamics of cortical myosin II (NMY-II::GFP) in wild-type (WT) and ect-2 ts embryos. Surface images are shown next to kymographs which depict flow during establishment, “early” maintenance, and “late” maintenance. (B) Distribution of myosin (top) and flow speed (bottom) during late maintenance in wild-type (black; 60 second interval before cytokinesis) and ect-2 ts (blue; 30 second interval before cytokinesis). Error bars indicate mean \pm 1 SEM for $n = 10$ embryos. (C) Dynamics of PAR-6 (PAR-6::GFP) in ect-2 ts embryos, without (left) and with (right) MRCK (RNAi) treatment. (D) Boundary position in nop-1 (RNAi) embryos, without (left) and with (right) MRCK (RNAi) treatment. (E) Dynamics of cortical myosin II (NMY-II::GFP) in wild-type (WT) and cdk-1 (RNAi) embryos. Kymographs and blue-boxed insets show patterns of cortical flow during maintenance. Graph shows the average myosin boundary position since pseudocleavage (PC) relaxation ($t = 0$) for wild type (red) and cdk-1(RNAi) (black) embryos (error bars are single sem for $n = 6$ (WT) and $n = 9$ (cdk-1(RNAi)) embryos; gray lines show individual CDK-1 (RNAi) embryo measurements).

Missing from this figure: PAR-6::GFP for ect-2 ts with and without PAR-6 RNAi (Cassandra).
 Nop-1 experiment: nop-1 mutant strain expressing PAR-2 and PAR-6. Show boundary position before and after maintenance with+without MRCK (RNAi) (Ed?).

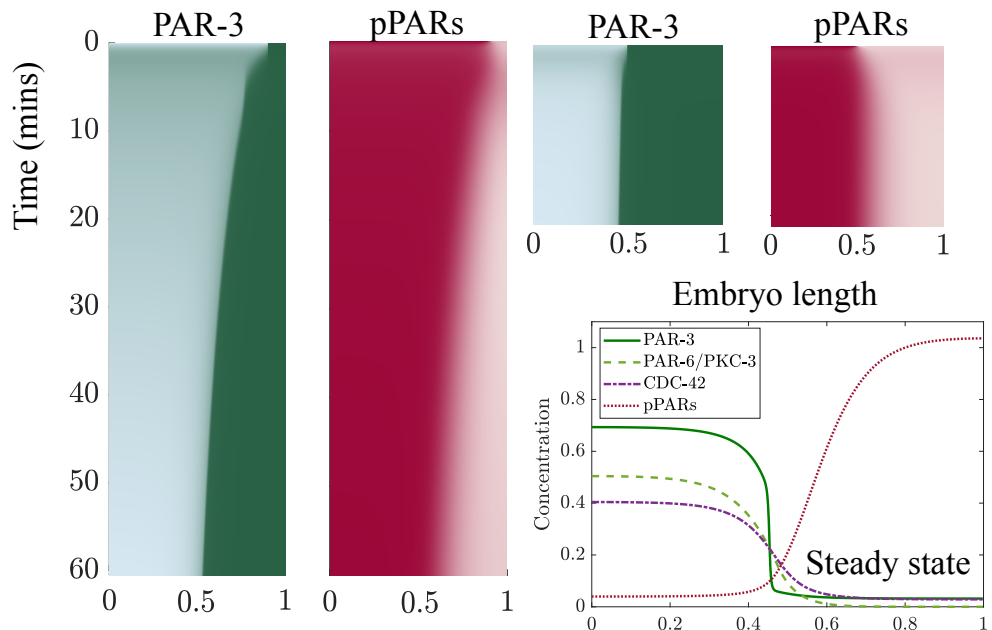
A Known Biochemistry Circuit



Simplified model



B Simulations without flow



C Simulations with flow

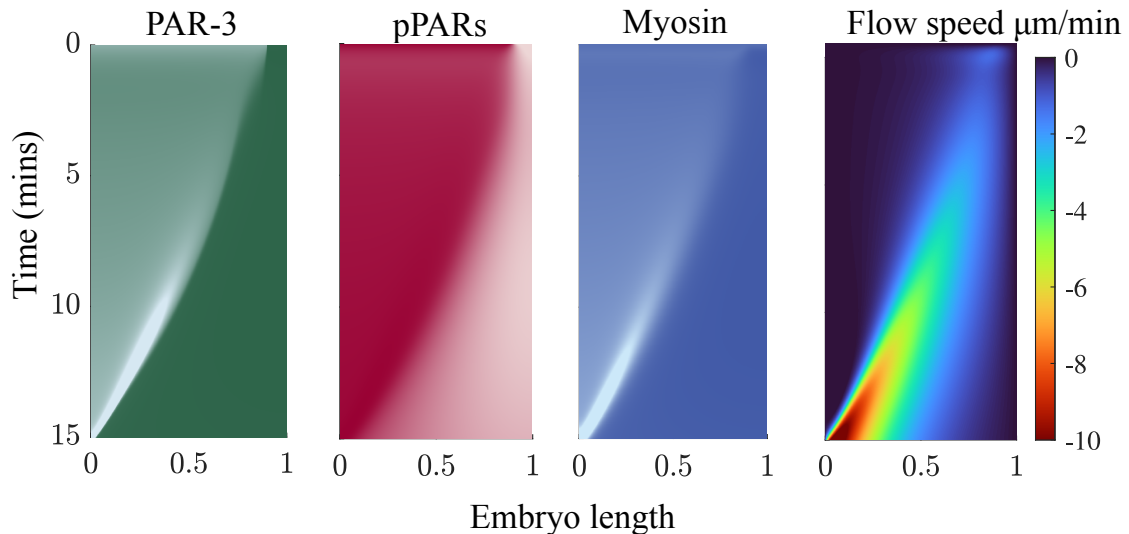


Figure 3: Models based a simple interaction of PAR proteins and myosin can stably maintain a polarity boundary, but cannot explain rescue. (A) Simplified model of PAR protein dynamics, and how it relates to the known system biochemistry (Lang and Munro, 2017). (B) Simulations without flow can maintain a stable boundary but cannot reproduce rescue in a realistic time. These panels show pseudo-kymographs of PAR-3 (green, left) and pPARs (red, right) in rescue (left, the boundary starts at 90% embryo length) and normal maintenance (right, the boundary starts at 50% embryo length) conditions. The bottom plot shows the unique steady state in the model without flow. (C) Simulations with flow lead to a vanishing anterior domain. Shown are pseudo-kymographs of the PAR-3, pPAR, and myosin concentrations over time, as well as the flow speeds.

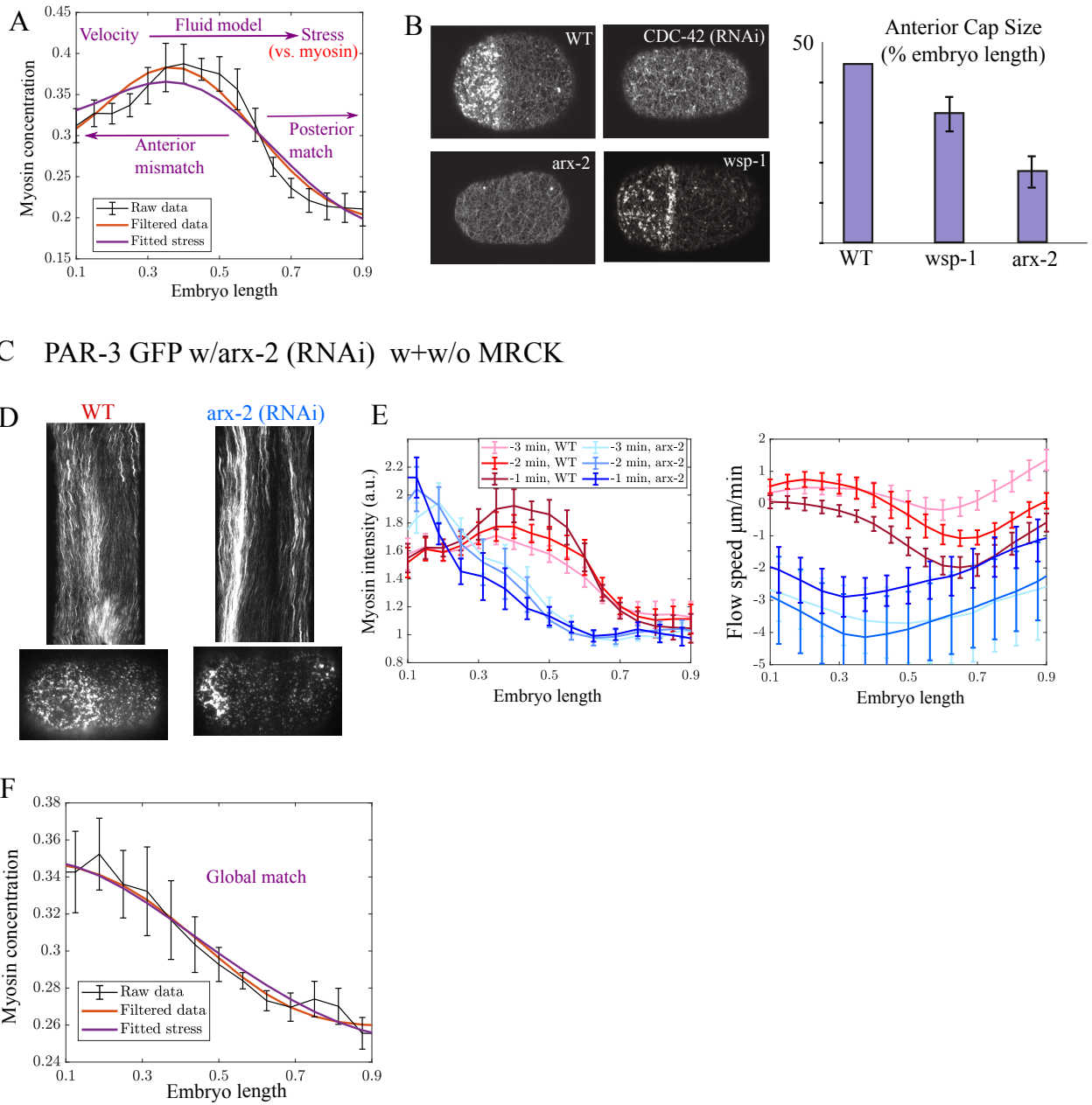


Figure 4: Branched actin acts in the anterior to suppress contractility in wild-type embryos.

Missing from this figure: (1) WASP (RNAi) – we should discuss if we can use Ed’s data for this(?), (2) arx-2 (RNAi) with MRCK (RNAi), PAR-3::GFP for (3) WT, (4) arx-2 (RNAi), (5) arx-2 (RNAi) with nocodazole. Do we need all of these?

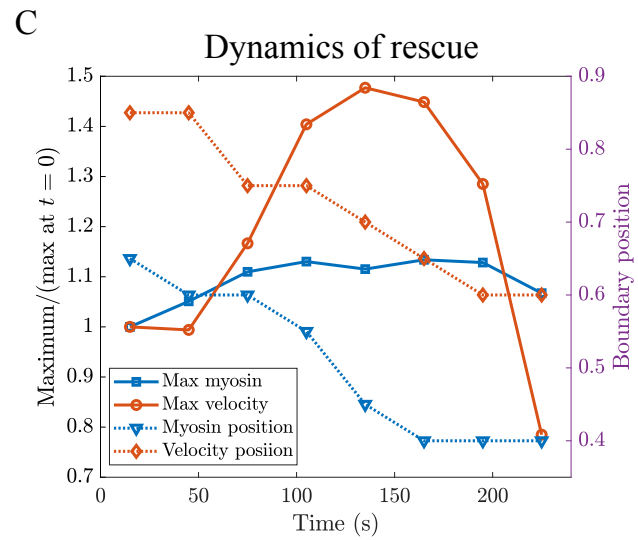
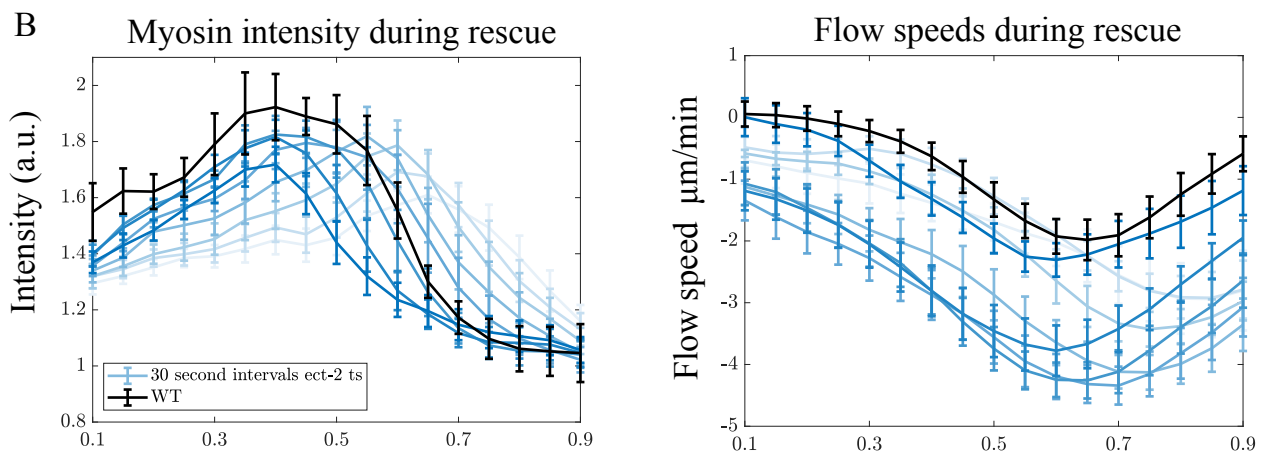
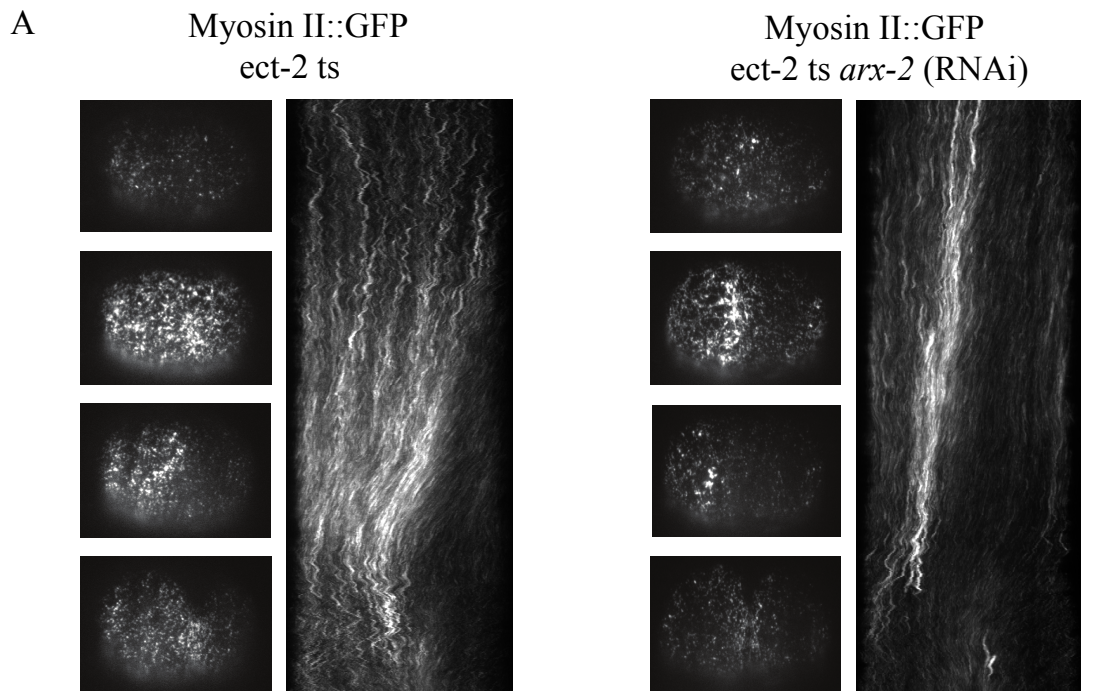


Figure 5: Branched actin acts suddenly to alleviate contractile tension in the anterior during maintenance phase rescue. (A) Surface views images and kymograph of myosin II (NMY-2::GFP) in ect-2 ts embryos (left) and ect-2 ts embryos with arx-2 (RNAi) (right). (B) Myosin intensity and flow speeds in ect-2 (ts) embryos (blue lines) compared to wild-type (black). Data are shown at 30 second intervals using progressively darker lines, and wild-type data in the last minute of maintenance phase are shown in black. Error bars show a single standard error in the mean ($n = 10$ for each condition). (c) Summary of rescue dynamics in ect-2 ts embryos. Solid lines, governed by the left axis, show the maximum in myosin intensity (blue) and velocity (red), averaged across $n = 10$ embryos and scaled by the value at the onset of maintenance phase ($t = 0$). Dashed lines, governed by the right axis, show the position of the peak in myosin (blue) and velocity (red) over time.

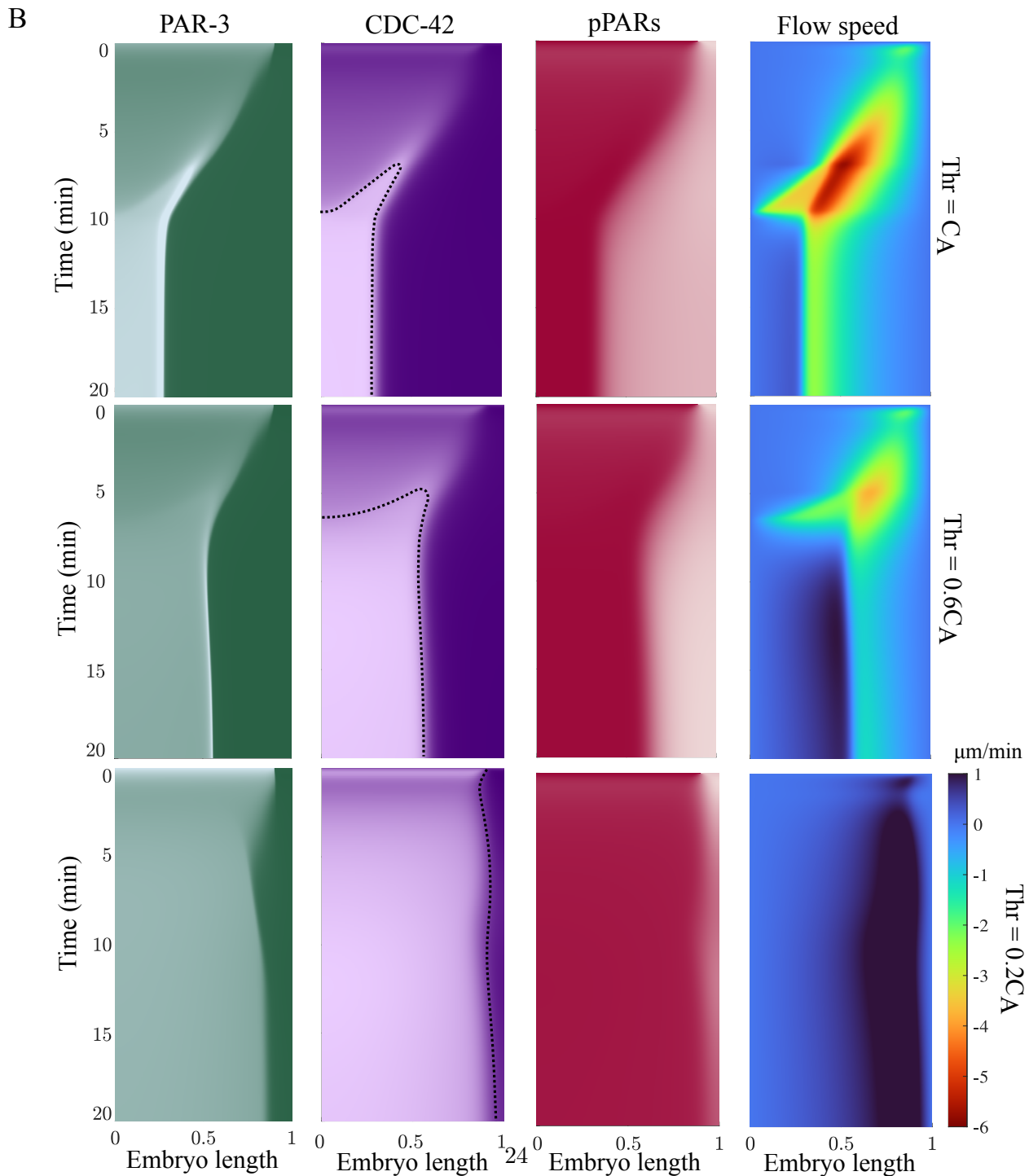
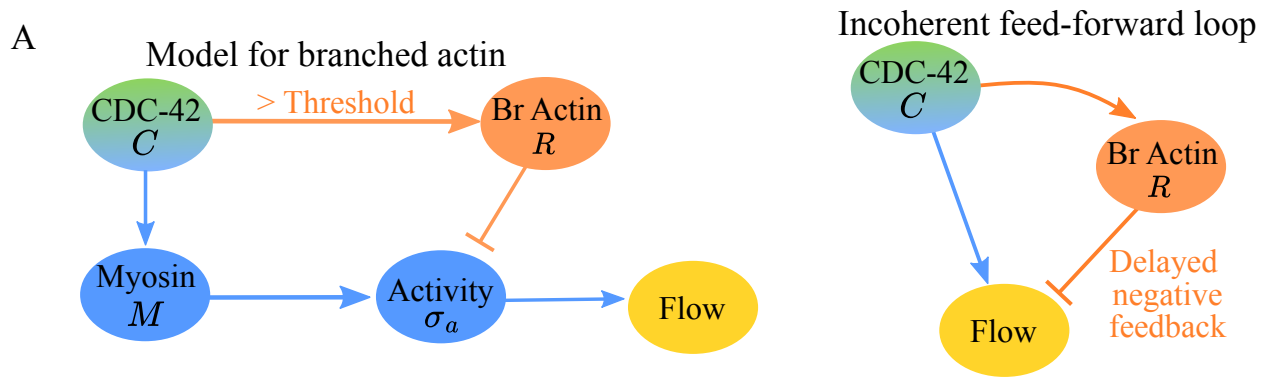


Figure 6: Models that incorporate branched actin successfully reproduce the dynamics of rescue. (A) Extension of the model presented in Fig. 3(A) to account for branched actin. Above a threshold of CDC-42, branched actin is produced and inhibits contractile stress (left). At its simplest level, these dynamics are an incoherent feed-forward loop (right). (B) Simulations with varying branched actin thresholds show varying degrees of contractility. Shown are kymographs of the PAR-3 concentration, CDC-42 concentration (the brighter region outlined in black is where the concentration is above the threshold for branched actin production), pPAR concentration, and flow speeds (all with the same scale bar given at bottom right) over time. Each row shows a different threshold for branched actin, given in terms of the typical anterior CDC-42 concentration without flows (denoted by C_A). The threshold decreases from C_A to $0.6C_A$ to $0.2C_A$ moving from top to bottom.

References

- Donato Aceto, Melissa Beers, and Kenneth J Kemphues. Interaction of par-6 with cdc-42 is required for maintenance but not establishment of par asymmetry in *c. elegans*. *Developmental biology*, 299(2):386–397, 2006.
- Tom Bland, Nisha Hirani, David Briggs, Riccardo Rossetto, KangBo Ng, Neil Q McDonald, David Zwicker, and Nathan W Goehring. Optimized dimerization of the par-2 ring domain drives cooperative and selective membrane recruitment for robust feedback-driven cell polarization. *bioRxiv*, pages 2023–08, 2023.
- Justin S Bois, Frank Jülicher, and Stephan W Grill. Pattern formation in active fluids. *Biophysical Journal*, 100(3):445a, 2011.
- Carrie R Cowan and Anthony A Hyman. Acto-myosin reorganization and par polarity in *c. elegans*. 2007.
- Adrian A Cuenca, Aaron Schetter, Donato Aceto, Kenneth Kemphues, and Geraldine Seydoux. Polarization of the *c. elegans* zygote proceeds via distinct establishment and maintenance phases. 2003.
- Adriana T Dawes and Edwin M Munro. Par-3 oligomerization may provide an actin-independent mechanism to maintain distinct par protein domains in the early *caenorhabditis elegans* embryo. *Biophysical journal*, 101(6):1412–1422, 2011.

Evan B Dewey, Danielle T Taylor, and Christopher A Johnston. Cell fate decision making through oriented cell division. *Journal of developmental biology*, 3(4):129–157, 2015.

Nathan W Goehring, Philipp Khuc Trong, Justin S Bois, Debanjan Chowdhury, Ernesto M Nicola, Anthony A Hyman, and Stephan W Grill. Polarization of par proteins by advective triggering of a pattern-forming system. *Science*, 334(6059):1137–1141, 2011.

Bob Goldstein and Ian G Macara. The par proteins: fundamental players in animal cell polarization. *Developmental cell*, 13(5):609–622, 2007.

Monica Gotta, Mary C Abraham, and Julie Ahringer. Cdc-42 controls early cell polarity and spindle orientation in *c. elegans*. *Current biology*, 11(7):482–488, 2001.

Peter Gross, K Vijay Kumar, Nathan W Goehring, Justin S Bois, Carsten Hoege, Frank Jülicher, and Stephan W Grill. Guiding self-organized pattern formation in cell polarity establishment. *Nature physics*, 15(3):293–300, 2019.

Niv Ierushalmi and Kinneret Keren. Cytoskeletal symmetry breaking in animal cells. *Current Opinion in Cell Biology*, 72:91–99, 2021.

Rukshala Illukkumbura, Nisha Hirani, Joana Borrego-Pinto, Tom Bland, KangBo Ng, Lars Huhbatsch, Jessica McQuade, Robert G Endres, and Nathan W Goehring. Design principles for selective polarization of par proteins by cortical flows. *Journal of Cell Biology*, 222(8), 2023.

Sukriti Kapoor and Sachin Kotak. Centrosome aurora a regulates rhogef ect-2 localisation and ensures a single par-2 polarity axis in *c. elegans* embryos. *Development*, 146(22):dev174565, 2019.

Amanda J Kay and Craig P Hunter. Cdc-42 regulates par protein localization and function to control cellular and embryonic polarity in *c. elegans*. *Current Biology*, 11(7):474–481, 2001.

Kerstin Klinkert, Nicolas Levernier, Peter Gross, Christian Gentili, Lukas von Tobel, Marie Pierron, Coralie Busso, Sarah Herrman, Stephan W Grill, Karsten Kruse, et al. Aurora a depletion reveals centrosome-independent polarization mechanism in *caenorhabditis elegans*. *Elife*, 8:e44552, 2019.

Kraig T Kumfer, Steven J Cook, Jayne M Squirrell, Kevin W Eliceiri, Nina Peel, Kevin F O’Connell, and John G White. Cgef-1 and chin-1 regulate cdc-42 activity during asymmetric division in the *caenorhabditis elegans* embryo. *Molecular biology of the cell*, 21(2):266–277, 2010.

Charles F Lang and Edwin Munro. The par proteins: from molecular circuits to dynamic self-stabilizing cell polarity. *Development*, 144(19):3405–3416, 2017.

Charles F Lang, Alexander Anneken, and Edwin Munro. Oligomerization and feedback on membrane recruitment stabilize par-3 asymmetries in *c. elegans* zygotes. *bioRxiv*, pages 2023–08, 2023.

Rong Li and Bruce Bowerman. Symmetry breaking in biology. *Cold Spring Harbor perspectives in biology*, 2(3):a003475, 2010.

Katrina M Longhini and Michael Glotzer. Aurora a and cortical flows promote polarization and cytokinesis by inducing asymmetric ect-2 accumulation. *Elife*, 11:e83992, 2022.

Jean-Léon Maître, Hervé Turlier, Rukshala Illukkumbura, Björn Eismann, Ritsuya Niwayama, François Nédélec, and Takashi Hiiragi. Asymmetric division of contractile domains couples cell positioning and fate specification. *Nature*, 536(7616):344–348, 2016.

Nadia I Manzi, Bailey N de Jesus, Yu Shi, and Daniel J Dickinson. Temporally distinct roles of aurora a in polarization of the *c. elegans* zygote. *Development*, 151(7):dev202479, 2024.

Mirjam Mayer, Martin Depken, Justin S Bois, Frank Jülicher, and Stephan W Grill. Anisotropies in cortical tension reveal the physical basis of polarizing cortical flows. *Nature*, 467(7315):617–621, 2010.

Ani Michaud, Marcin Leda, Zachary T Swider, Songeun Kim, Jiaye He, Jennifer Landino, Jenna R Valley, Jan Huisken, Andrew B Goryachev, George von Dassow, et al. A versatile cortical pattern-forming circuit based on rho, f-actin, ect2, and rga-3/4. *Journal of Cell Biology*, 221(8):e202203017, 2022.

Jonathan B Michaux, François B Robin, William M McFadden, and Edwin M Munro. Excitable rhoa dynamics drive pulsed contractions in the early *c. elegans* embryo. *Journal of Cell Biology*, 217(12):4230–4252, 2018.

Yoichiro Mori, Alexandra Jilkine, and Leah Edelstein-Keshet. Wave-pinning and cell polarity from a bistable reaction-diffusion system. *Biophysical journal*, 94(9):3684–3697, 2008.

Fumio Motegi and Asako Sugimoto. Sequential functioning of the ect-2 rhogef, rho-1 and cdc-42

establishes cell polarity in *caenorhabditis elegans* embryos. *Nature cell biology*, 8(9):978–985, 2006.

Fumio Motegi, Seth Zonies, Yingsong Hao, Adrian A Cuenca, Erik Griffin, and Geraldine Seydoux. Microtubules induce self-organization of polarized par domains in *caenorhabditis elegans* zygotes. *Nature cell biology*, 13(11):1361–1367, 2011.

Edwin Munro and Bruce Bowerman. Cellular symmetry breaking during *caenorhabditis elegans* development. *Cold Spring Harbor perspectives in biology*, 1(4):a003400, 2009.

Edwin Munro, Jeremy Nance, and James R Priess. Cortical flows powered by asymmetrical contraction transport par proteins to establish and maintain anterior-posterior polarity in the early *c. elegans* embryo. *Developmental cell*, 7(3):413–424, 2004.

Camelia G Muresan, Zachary Gao Sun, Vikrant Yadav, A Pasha Tabatabai, Laura Lanier, June Hyung Kim, Taeyoon Kim, and Michael P Murrell. F-actin architecture determines constraints on myosin thick filament motion. *Nature communications*, 13(1):7008, 2022.

Masatoshi Nishikawa, Sundar Ram Naganathan, Frank Jülicher, and Stephan W Grill. Controlling contractile instabilities in the actomyosin cortex. *Elife*, 6:e19595, 2017.

Alice Y Pollitt and Robert H Insall. Wasp and scar/wave proteins: the drivers of actin assembly. *Journal of cell science*, 122(15):2575–2578, 2009.

Jacob D Reich, Lars Hubatsch, Rukshala Illukkumbura, Florent Peglion, Tom Bland, Nisha Hirani, and Nathan W Goehring. Regulated activation of the par polarity network ensures a timely and specific response to spatial cues. *Current Biology*, 29(12):1911–1923, 2019.

François B Robin, William M McFadden, Baixue Yao, and Edwin M Munro. Single-molecule analysis of cell surface dynamics in *caenorhabditis elegans* embryos. *Nature methods*, 11(6):677–682, 2014.

Josana Rodriguez, Florent Peglion, Jack Martin, Lars Hubatsch, Jacob Reich, Nisha Hirani, Alicia G Gubieda, Jon Roffey, Artur Ribeiro Fernandes, Daniel St Johnston, et al. apkc cycles between functionally distinct par protein assemblies to drive cell polarity. *Developmental cell*, 42(4):400–415, 2017.

Anne Sailer, Alexander Anneken, Younan Li, Sam Lee, and Edwin Munro. Dynamic opposition of clustered proteins stabilizes cortical polarity in the *c. elegans* zygote. *Developmental cell*, 35(1):131–142, 2015.

Stephanie Schonegg and Anthony A Hyman. Cdc-42 and rho-1 coordinate acto-myosin contractility and par protein localization during polarity establishment in *c. elegans* embryos. 2006.

Lawrence E Small and Adriana T Dawes. Par proteins regulate maintenance-phase myosin dynamics during *caenorhabditis elegans* zygote polarization. *Molecular biology of the cell*, 28(16):2220–2231, 2017.

Yu Chung Tse, Michael Werner, Katrina M Longhini, Jean-Claude Labbe, Bob Goldstein, and Michael Glotzer. Rhoa activation during polarization and cytokinesis of the early *caenorhabditis elegans* embryo is differentially dependent on *nop-1* and *cyk-4*. *Molecular biology of the cell*, 23(20):4020–4031, 2012.

Qing Yang, Xiao-Feng Zhang, Thomas D Pollard, and Paul Forscher. Arp2/3 complex-dependent actin networks constrain myosin ii function in driving retrograde actin flow. *Journal of Cell Biology*, 197(7):939–956, 2012.

Baixue Yao, Seth Donoughe, Jonathan Michaux, and Edwin Munro. Modulating rhoa effectors induces transitions to oscillatory and more wavelike rhoa dynamics in *caenorhabditis elegans* zygotes. *Molecular Biology of the Cell*, 33(6):ar58, 2022.

Seth Zonies, Fumio Motegi, Yingsong Hao, and Geraldine Seydoux. Symmetry breaking and polarization of the *c. elegans* zygote by the polarity protein par-2. *Development*, 137(10):1669–1677, 2010.